Applied Surface Science 333 (2015) 220–228

Contents lists available at ScienceDirect

Applied Surface Science

journal homepage: www.elsevier.com/locate/apsusc

Rapid reductive degradation of aqueous p-nitrophenol using nanoscale zero-valent iron particles immobilized on mesoporous silica with enhanced antioxidation effect

Lin Tang[a,b,*], Jing Tang[a,b], Guangming Zeng[a,b,*], Guide Yang[a,b], Xia Xie[a,b], Yaoyu Zhou[a,b], Ya Pang[c], Yan Fang[a,b], Jiajia Wang[a,b], Weiping Xiong[a]

[a] College of Environmental Science and Engineering, Hunan University, Changsha, Hunan 410082, PR China
[b] Key Laboratory of Environmental Biology and Pollution Control, Hunan University, Ministry of Education, Changsha 410082, PR China
[c] Department of Biological Engineering and Environmental Science, Changsha College, Changsha 410003, PR China

ARTICLE INFO

Article history:
Received 21 October 2014
Received in revised form 14 January 2015
Accepted 3 February 2015
Available online 10 February 2015

Keywords:
Nanoscale zero-valent iron
Mesoporous silica
p-Nitrophenol
Reduction

ABSTRACT

In this study, nanoscale zero-valent iron particles immobilized on mesoporous silica (nZVI/SBA-15) were successfully prepared for effective degradation of p-nitrophenol (PNP). The nZVI/SBA-15 composites were characterized by N_2 adsorption/desorption, transmission electron microscopy (TEM), UV–vis spectrum and X-ray photoelectron spectroscopy (XPS). Results showed that abundant ultrasmall nanoscale zero-valent iron particles were formed and well dispersed on mesoporous silica (SBA-15). Batch experiments revealed that PNP removal declined from 96.70% to 16.14% as solution pH increased from 3.0 to 9.0. Besides, degradation equilibrium was reached within 5 min, which was independent of initial PNP concentration. Furthermore, only a little PNP elimination on SBA-15 indicated that nZVI immobilized on mesoporous silica was mainly responsible for the target contaminant removal. The UV–vis spectrum and XPS measurement confirmed that the PNP removal was a reductive degradation process, which was further proved by the detected intermediates using gas chromatography–mass spectrometry (GC/MS). The excellent antioxidation ability had been discovered with more than 80% of PNP being removed by nZVI/SBA-15 treated with 30 days' exposure to air. These results demonstrated the feasible and potential application of nZVI/SBA-15 composites in organic wastewater treatment.

1. Introduction

The concern for public health and environmental safety has been increasing over the last few decades. Chemical pollution of surface water poses a threat on the aquatic environment with hazardous effects [1]. As we know, nitroaromatic compounds (NACs) have been widely applied in industry and agriculture, which are used as pesticides, polymers, pharmaceuticals, and intermediates in synthesis of dyes [2–5]. As a species of NACs, p-nitrophenol (PNP) is a kind of dangerous substance with cumulative effects and can invade the body through the respiratory system, digestive system and skin [6]. Besides, PNP can damage DNA or inhibit the synthesis of DNA, which would cause major adverse effects on the blood, liver and central nervous system. Thus, it is necessary to develop an efficient treatment process to decompose this refractory and toxic pollutant. Up to now, there are many techniques for the degradation of p-nitrophenol in wastewater, such as advance oxidation process (AOPs) [7], extraction [8], adsorption [9] and reduction [10,11]. As a reductive agent, nanoscale zero-valent iron (nZVI) has recently been used to treat the toxic and refractory pollutants such as metals [12], organochlorine compounds [13] and nitroaromatic compounds [14]. Due to its high surface area, abundant reactive surface sites, high reaction rate and injectability into aquifers [15], nZVI has gained extensive attention. However, the aggregation of nZVI limits its dispersibility and mobility in effluents, and the oxidization of nZVI can significantly decrease its reactivity [16,17]. Therefore, it is necessary to solve these problems for application. Recently, immobilization of nZVI on some porous materials, like multiwalled carbon nanotubes [18], zeolite [19], activated carbon [20], bentonite [21], mesoprous carbon [22] and SBA-15 [23,24], is considered as an alternative solution to solve these troubles.

In recent years, an impregnation technique named "two solvents" method has aroused researchers' interest [23–25]. Sun et al. [24] used a hydrophobic alkane solvent (cyclohexane) to prewet the

* Corresponding authors at: College of Environmental Science and Engineering, Hunan University, Changsha, Hunan 410082, PR China. Tel.: +86 731 88822778; fax: +86 731 88823701.
E-mail addresses: tanglin@hnu.edu.cn (L. Tang), zgming@hnu.edu.cn (G. Zeng).

http://dx.doi.org/10.1016/j.apsusc.2015.02.025
0169-4332/

surfaces of SBA-15 before addition of iron precursor aqueous solutions, and the synthesized nZVI dispersed well on SBA-15. Thus, this impregnation method has been confirmed to be efficient in hosting nZVI on porous materials.

In this paper, we successfully prepared nZVI/SBA-15 composites utilizing the "two solvents" technique with n-pentane, instead of cyclohexane, as hydrophobic alkane solvent. Owing to the lower boiling temperature of n-pentane, the preparation procedure of nZVI/SBA-15 obviously was cut down, which would simplify these processes. Pentane had lower interfacial tension with water, which could possibly result in the easier formation of smaller droplets of aqueous solution [26,27]. Although with lower interfacial tension, water droplets in oil would have more chances to agglomerate, they might remain dispersed to form smaller nanoparticles in the silica channels with our "two solvents" method. The prepared nZVI/SBA-15 was characterized by transmission electron microscopy (TEM) and nitrogen adsorption–desorption isotherms. For the first time, the resultant solid was applied to remove organic matters, such as PNP, from aqueous solutions. The effects of relevant parameters such as solution pH, initial concentration of PNP and contact time on the degradation efficiency of PNP by nZVI/SBA-15 were investigated. UV–vis spectrum, X-ray photoelectron spectroscopy (XPS) and gas chromatography–mass spectrometry (GC/MS) analysis of composites were applied to further analyze the mechanism of PNP degradation. In addition, the leaching of iron ions from nZVI/SBA-15 into the solution was also investigated. Finally, we compared the removal efficiency of PNP by bare nanoscale zero-valent iron particles and the composites after exposing to air to examine their antioxidation abilities. It is worth mentioning that the antioxidation activity of nZVI/SBA-15 has not been studied before.

2. Materials and experimental methods

2.1. Materials and chemicals

Pluronic copolymer P123 (EO20PO70EO20, EO = ethylene oxide, PO = propylene oxide) was purchased from Sigma–Aldrich (USA), and all reagents used in the experiment were of analytical reagent grade except that dichloromethane was of chromatographic reagent grade. What's more, all solutions were prepared with high-purity water (18.25 MΩ/cm) from a Milli-Q water purification system.

2.2. Preparation of nZVI/SBA-15 and nZVI

SBA-15 was synthesized as described by Zhao et al. [28]. The nZVI/SBA-15 composites were similarly prepared by a "two solvents" method at room temperature reported in Refs. [24,26]. Briefly, with the magnetic stirring, 1.0 g SBA-15 was mixed with 30 mL n-pentane followed by adding dropwise a small volume of ferrous aqueous solution which contained 1.112 g iron sulfate heptahydrate. The mixture evaporated at 60 °C for one night. Then, under the N_2 protection condition, Fe (II) or Fe (III) impregnated SBA-15 were reduced to metallic Fe^0 in the 30 mL n-pentane solvent by adding 8 mL $NaBH_4$ solution (2 M) with stirring. The obtained composites were separated from the solution by a magnet, washed with methanol three times, and then dried in vacuum at 50 °C for one day.

Comparatively, nZVI was also prepared. 4.0 g $FeSO_4{\cdot}7H_2O$ dissolved in 200 mL methanol and deoxygenated water mixture (30% v/v). Soon afterwards, under the N_2 protection condition, 10 mL $NaBH_4$ solution (2.1 M) was added dropwise in aforementioned solution with mechanical stirring, which was kept reacting for 30 min. After filtration and then washing the separated black solid with ethanol, the nZVI was dried in vacuum at 50 °C for one day.

2.3. Characterizations

The morphological images were obtained on a FEI Tecnai G2 20 transmission electron microscope (TEM) operated at 100 kV. Nitrogen adsorption–desorption isotherms were measured on Micromeritics 2020 analyzer at 77.3 K. BET analyses were applied to determine the surface area. BJH analyses were used to derive pore size distribution and calculate the total pore volume. An X-ray photoelectron spectroscopy (XPS) (Thermo Fisher Scientific) was utilized to measure the surface composition and the elements' valence of nZVI/SBA-15 before and after reaction with a resolution of 0.5 eV.

2.4. Batch experiments

All batch experiments were performed in glass conical flasks undergoing shaking at 150 rpm at 25 °C, and the solution pH was adjusted with 0.1 mol/L NaOH or 0.1 mol/L HCl. 0.05 g nZVI/SBA-15 or SBA-15 was added into 10 mL PNP solution for each treatment unless otherwise stated. Then, aliquots of the aqueous solutions were withdrawn by a syringe at intervals, and finally filtered by a 0.2 μm membranes filter to separate the solid from the liquid. The antioxidation ability of nZVI/SBA-15 and nZVI were investigated by exposure to the air for 0 day, 3 days, 7 days, 14 days, 21 days and 30 days, respectively. All the experiments were carried out in duplicate, and the averages were calculated.

2.5. Analytical methods

The residual concentration of the pollutant was determined by UV–vis spectroscopy (SHIMADZU 2550) in acidic form at maximum absorbing wavelength (λ = 315 nm) [29]. The concentration of PNP was measured at pH in the range from 1 to 3 to ensure that only one form of the compound existed in the solution. What's more, the UV–vis absorption spectrum of the treated pollutant were carried out in quartz cuvettes, and the UV–vis spectrum were recorded from 190 to 800 nm using HCl solutions with the same concentration.

The concentration of total leaching iron ions of the composites in the solution was determined by a Perkin-Elmer Analyst 700 atomic absorption spectrophotometer (AAS, Perkin-Elmer, USA).

In addition, a gas chromatography–mass spectrometry (GC/MS) analytical method was set up to qualitatively determine the degradation intermediate products of PNP [30]. Before GC/MS determination, 50 mL sample was extracted using 10 mL dichloromethane for three times under acidic (pH 2.0), neutral (pH 7.0), alkaline (pH 12.0) conditions, respectively. The three extracted layers were mixed up, and then dehydrated with anhydrous sodium sulfate. Under nitrogen atmosphere, the mixture was dried at the room temperature. Subsequently, the residue was dissolved in 1.0 mL CH_2Cl_2, and 1 μL of the liquid was injected into a QP2010-PLUS GC/MS system (SHIMADZU, Japan) equipped with a HP-5MS capillary column. The GC column was operated in a temperature program mode beginning at 40 °C for 3 min, rising by 10 °C/min to 280 °C, and holding at 280 °C for 5 min. The solvent delay was 6 min, and the total run time was 32 min. The mass range scanned was 20–500 *m/z*.

3. Results and discussion

3.1. Characterization of materials

Fig. 1 showed the transmission electron microscopy (TEM) images of SBA-15, nZVI/SBA-15 and nZVI. The TEM images in Fig. 1a–d indicated that both the two mesoporous materials had

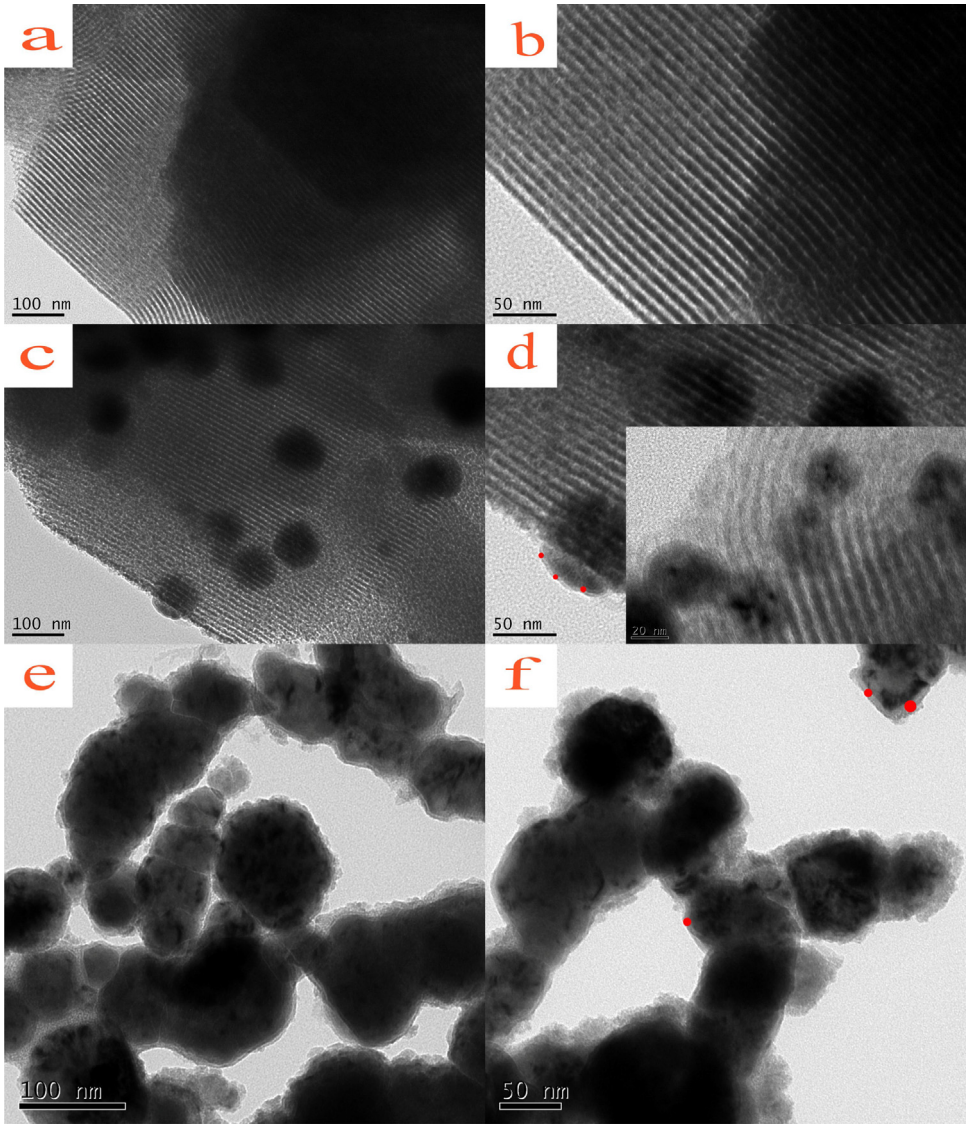

Fig. 1. TEM images of SBA-15 (a, b), nZVI/SBA-15 (c, d) and nZVI (e, f). Insert: HR-TEM images of nZVI/SBA-15 with resolution of 20 nm.

rodlike morphology, and the ordered stripe-like structures of mesopores were clearly observed for the two mesoporous silicas [31]. However, the degree of order was slightly lower for nZVI/SBA-15 especially in Fig. 1d insert, which demonstrated some deteriorations of the mesoporous structure after introduction of iron. As a result of preparation with "two solvents" method, a part of iron nanoparticles with minor diameter were embedded in channels [26,32]. Nevertheless, for nZVI/SBA-15 (Fig. 1c), many nanoscale iron particles with average size of approximately 50 nm were mainly dispersed on external surface of silica other than dispersing inside the channels. It appeared to be different from the composites reported by Sun et al. [24,26]. It might be because that many excess droplets of iron solution remained on the external surface of SBA-15 silica, and then they were agglomerated. Generally speaking, those big dots in Fig. 1c and d rarely formed chains, unlike the big particles in Fig. 1e and f. Besides, the non-incorporated nZVI (Fig. 1e) was spherical and aggregated with average size between 60 and 80 nm. Moreover, both the immobilized nZVI (Fig. 1d) and non-incorporated nZVI (Fig. 1f) were covered with iron oxide film whose thickness was shown by red dot marks with different diameters, which showed that the iron oxide film on immobilized nZVI was thinner than that on the bare nZVI [16]. The phenomenon indicated that these dispersive nanoparticles might be caused by the preparation processes, such as different stirring rate or the existence of hydrophobic alkane.

The isotherm curves of mesoporous silica and nZVI/SBA-15 (Fig. 2) exhibited the representative type-IV curves with hysteresis loops in the P/P_0 range 0.7–0.9, indicating that their structures were uniform mesoporous [33]. The corresponding pore size distributions (Fig. 2 insert) demonstrated that the two materials possessed a pore size distribution centered near 9.7 nm. The introduction of iron also led to a distinct decrease in BET surface area (from 375.212 to 160.867 m^2/g). This decrease might be ascribed to iron entering into the mesoporous channels, partially occupying or even blocking mesopores.

3.2. The influence of solution pH

Fig. 3 described the iron leaching amount of nZVI/SBA-15, and the removal efficiencies of PNP by nZVI/SBA-15 and bare mesoporous silica under different pH conditions. The amount of iron leaching through nZVI/SBA-15 descended substantially when the solution pH was above 2, and the highest amount of iron leaching was 168 mg/L when the solution pH was 2. Therefore, apart from

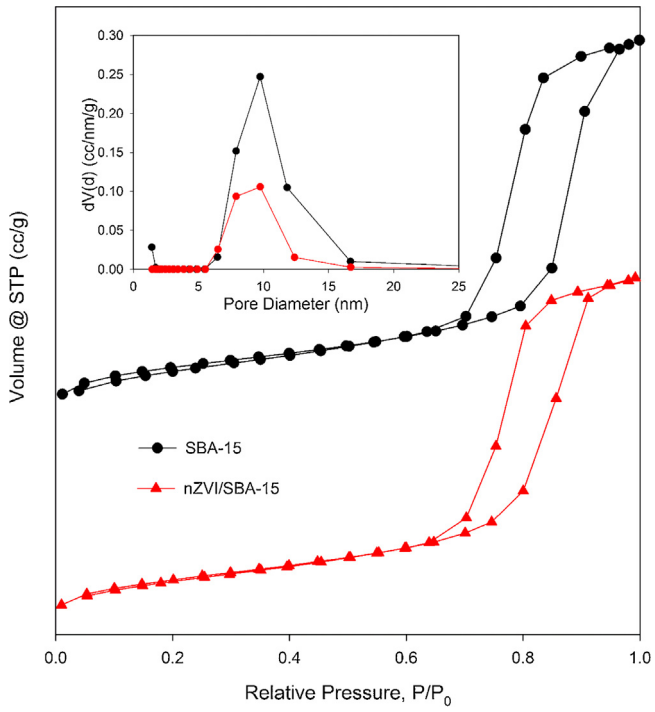

Fig. 2. Nitrogen adsorption–desorption isotherms of nZVI/SBA-15 and SBA-15. Insert: Pore size distribution of nZVI.SBA-15 and SBA-15.

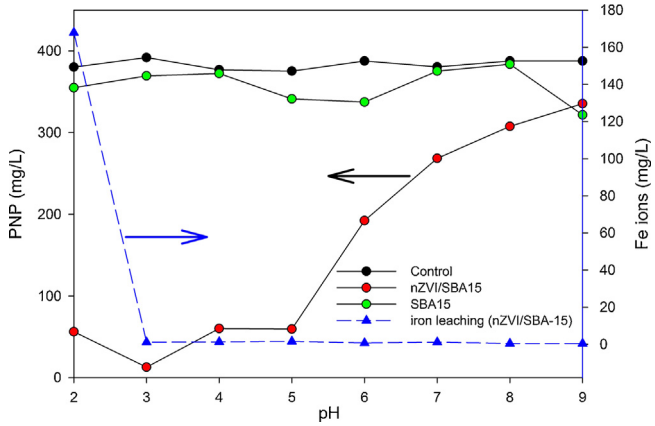

Fig. 3. Effect of pH values on iron leaching of nZVI/SBA-15 and the residual PNP concentration treated by nZVI/SBA-15 and SBA-15. Reaction conditions: 400 mg/L PNP removed on nZVI/SBA-15 and SBA-15 with concentration of 5 g/L at 25 °C, 150 rpm, within 240 min.

heavily acidic conditions, the leaching of iron had inconsiderable impact on its application in the aqueous environment.

Comparing the removal efficiencies of the two mesoporous materials for PNP, the bare mesoporous silica showed poor removal efficiency on the target pollutant. The high removal efficiency by nZVI/SBA-15 was probably related to the nZVI on the surface of mesoporous matrix. On the other hand, the removal efficiency by nZVI/SBA-15 was fairly high in the moderate strong acidic pH, and it could even reach 96% at pH 3. Subsequently, it decreased gradually with increasing of pH, and only 16% PNP removal efficiency was obtained at pH 9. The reason for this phenomenon might be that the H^+ participated in degrading PNP by nZVI/SBA-15. At solution pH lower than 3, the concentration of H^+ was so high that H^+ reacted with the materials directly and occupied the dominant position in the competition. In this process, H^+ received electrons by the corrosion of metallic iron and then produced hydrogen, which caused

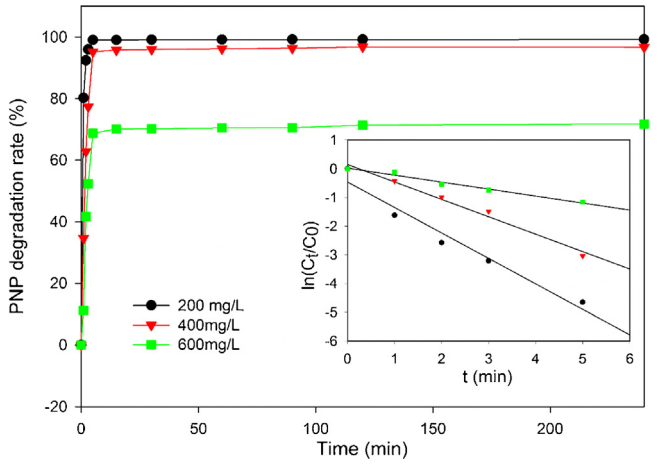

Fig. 4. Effect of initial PNP concentration and contact time on the PNP degradation rate by nZVI/SBA-15. Insert: Linear fitting using pseudo-first-order model. Reaction conditions: PNP removed on nZVI/SBA-15 with concentration of 5 g/L at 25 °C, 150 rpm.

the high concentration of iron ions in the solution. At the same time, it inhibited the PNP degradation reaction to a certain degree. With the pH slightly increasing, the amount of H^+ decreased and was insufficient to restrain the PNP removal. Thus, the PNP removal efficiency increased a bit. As the solution pH continued to increase, even at alkaline pH, the surface of metallic iron would be covered by iron oxide hydroxide, which hindered the PNP molecules from contacting with zero-valent iron particles, and thus the PNP removal dramatically decreased [34].

3.3. Kinetics study of PNP degradation

The reactivities of nZVI/SBA-15 for three different initial PNP concentrations (200, 400 and 600 mg/L) were investigated at pH 3. As shown in Fig. 4, the PNP removal equilibrium was reached within 5 min, and the degradation rate decreased with initial PNP concentration increasing. Kinetic model was applied to estimate the degradation mechanism in the initial stage (0–5 min). According to some literatures, the reduction of PNP by nZVI/SBA-15 was a solid–liquid inter-phase reaction, which agreed with the pseudo first-order kinetics model [16,35]. Therefore, the

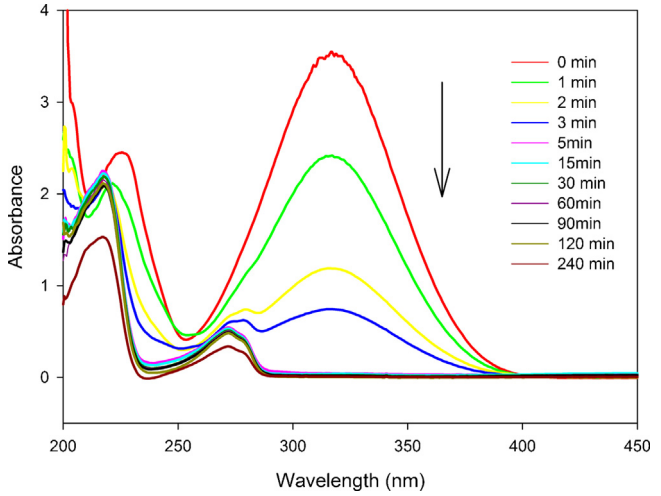

Fig. 5. UV–vis spectra of the influent and effluent of nZVI/SBA-15 with different treatment time. Reaction: 400 mg/L PNP removed on nZVI/SBA-15 with concentration of 5 g/L at 25 °C, 150 rpm, within 240 min.

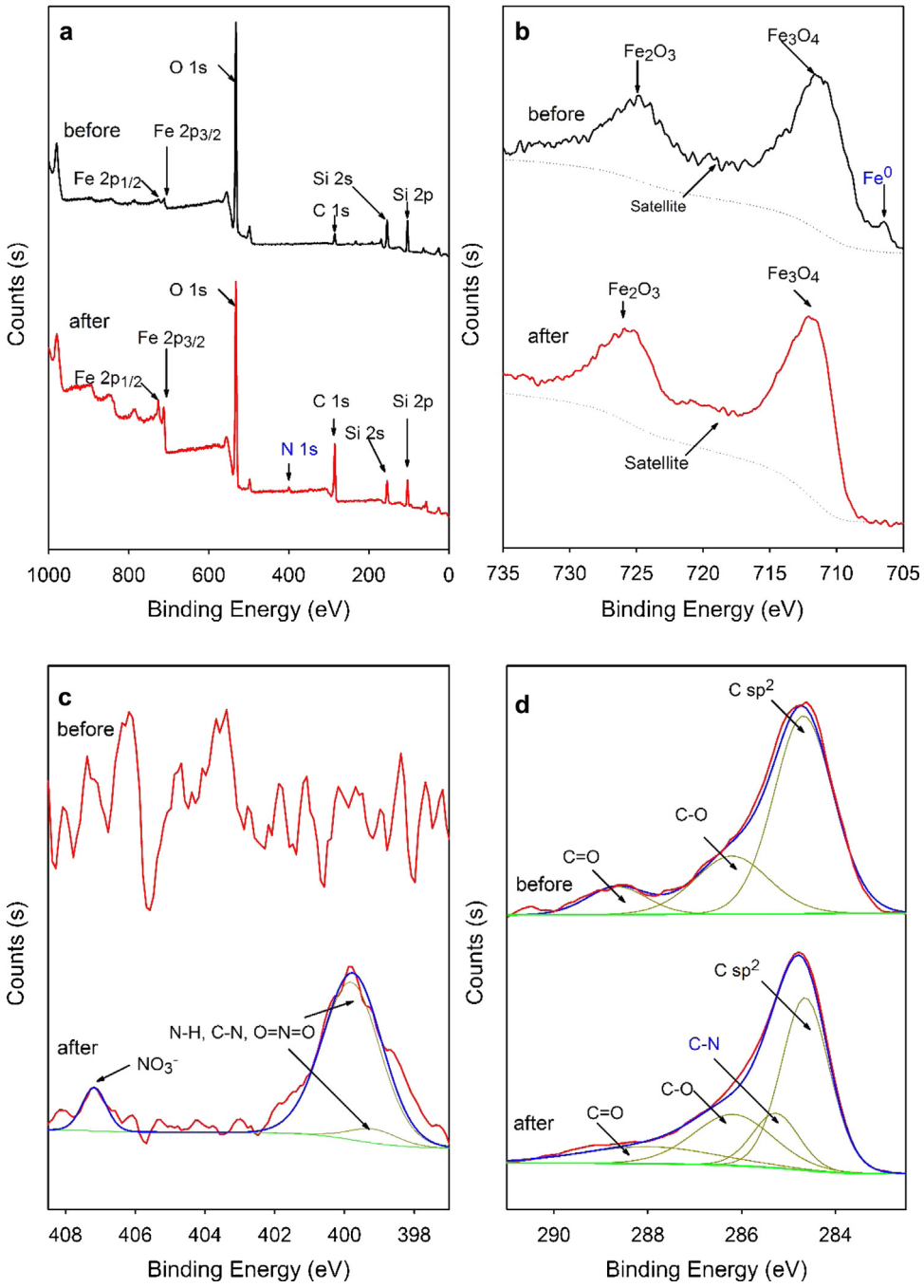

Fig. 6. XPS whole survey (a) and detailed XPS surveys of the regions for Fe 2p (b), N 1s (c) and C 1s (d) for nZVI/SBA-15 before and after reacting with 400 mg/L PNP.

pseudo-first-order was utilized to fit the experimental data [30]. The kinetic rate equation is expressed in Eq. (1):

$$\ln \frac{C_t}{C_0} = -K_{obs} t \quad (1)$$

where C_t and C_0 (mg/L) are the residual concentration of PNP at time t and the initial concentration, respectively; K_{obs} (min^{-1}) is the apparent rate constant.

A plot of natural logarithmic C_t/C_0 versus the reaction time was shown in Fig. 4 insert, and the values of the constant K_{obs} and correlation coefficients R^2 were calculated and given in Table 1. The linear relationships between C_t/C_0 and t had relatively high correlation coefficients, except for the plot with PNP initial concentration of 200 mg/L, since the target pollutant removal was too fast to accurately detect the residual PNP concentration at interval time. In brief, the removal processes were well fitted by the pseudo-first-order model, which indicated that the K_{obs} was reverse proportional to the initial concentration of PNP, and K_{obs} could be cut down by elevating the initial concentration of PNP. In addition, it was found that the apparent rate constant for

Table 1
Pseudo-first-order model parameters for PNP removal by nZVI/SBA-15.

Concentration (mg/L)	Apparent rate constant (K_{obs})	Correlation coefficients (R^2)
200	0.8875	0.9610
400	0.6075	0.9843
600	0.2432	0.9787

600 mg/L PNP was 0.2432 min^{-1}, which was much lower than that for other concentrations (0.8875 min^{-1} for 200 mg/L, 0.6075 min^{-1} for 400 mg/L). It could be explained from two aspects: (a) the active sites of composites were insufficient for the higher initial PNP concentration, markedly decreasing the removal of PNP; (b) the increase of initial PNP concentration would accelerate the competition among PNP and its intermediate products for the active sites of materials, which would affect the removal of PNP.

3.4. UV–vis spectra and XPS analysis

In order to observe visually the residual PNP concentration at different contact time, the UV–vis spectrum of the influent and effluent of nZVI/SBA-15 system with different treatment time (0–240 min) were presented in Fig. 5. The peak at 315 nm was mainly due to the conjugation of benzene ring and chromophonic group (i.e., $-NO_2$) [36]. It was observed that absorbance intensity of the peak at 315 nm decreased sharply in 240 min, which indicated that the $-NO_2$ group on the molecular structure of PNP was reduced effectively by nZVI/SBA-15.

Moreover, X-ray photoelectron spectroscopy (XPS) was applied to study the surface chemical compositions of the composites, and the results were shown in Fig. 6. Fig. 6a presented the whole region scan of the nZVI/SBA-15 surface before and after treated with the aqueous solution containing 400 mg/L PNP at initial pH 3 and 25 °C. For pure nZVI/SBA-15, the principal elements on the surface were oxygen, silicon, carbon and iron. The presence of carbon observed on the nZVI/SBA-15 surface was possibly resulted from an exposure to carbon dioxide from air and the pretreatment by organic solvent [37]. A new peak in the binding energy about 399.8 eV appeared after contact with PNP for 4 h, which stood for the existence of nitrogen [38]. In comparison, a more intense peak of carbon (284.7 eV) was shown in Fig. 6a demonstrating the attachment of various products to the composites.

Detailed XPS surveys of the regions for Fe 2p, N 1s and C 1s of the nZVI/SBA-15 surface before and after treatments were shown in Fig. 6b–d, respectively. For Fe 2p spectra, according to previous studies [32], the 711 and 725 eV binding energy of Fe 2p could be assigned to Fe_3O_4 and Fe_2O_3, respectively; and the satellite between two dominant peaks was due to a shake-up process by Fe^{2+} [37]. In addition, the peak at 706.6 eV was corresponded to Fe^0 [32] and then disappeared after reaction with nZVI/SBA-15, which was possibly due to the oxidation of the surface Fe^0 in the degradation process. In Fig. 6c, three peaks of curve-fitting for N 1s spectrum after treatments corresponding to NO_3^- (BE = 407.1 eV) and N–H, C–N or O=N=O (BE = 399.2 or 399.8 eV) were observed [39,40]. The presence of N–H was possibly related to the reduction action between nZVI with nitro-group of PNP. Further studies suggested that NO_3^- combined with Fe^{3+} to form $Fe_2(NO_3)_3$ [40]. For C 1s spectra (shown in Fig. 6d), there were three similar peaks of curve-fitting assigned to sp^2 carbons (C=C, C–C or C–H, BE = 284.7 eV), carbon coordinated to a single oxygen in hydroxyl groups or ethers

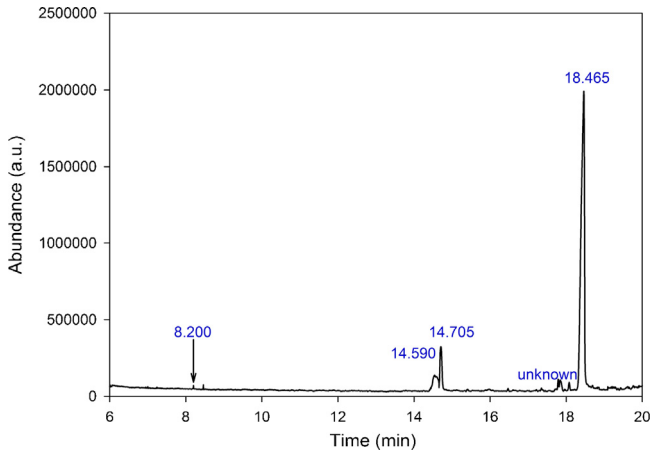

Fig. 7. GC–MS chromatograms on dichloromethane extract from the treatment effluent of nZVI/SBA-15.

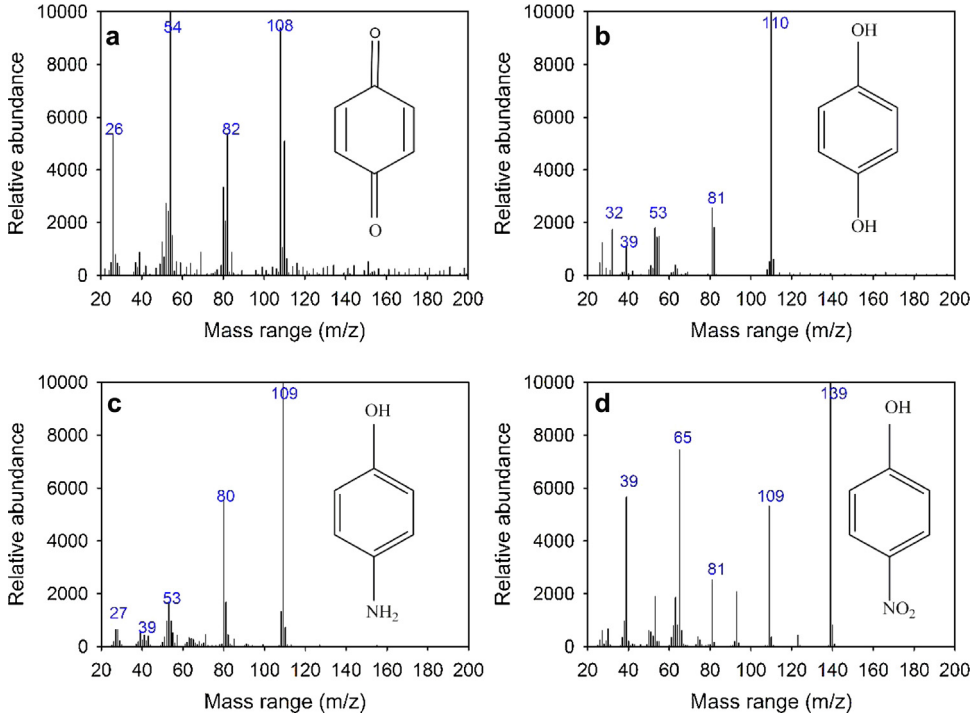

Fig. 8. Mass chromatogram of p-nitrophenol and the detected degradation products of p-nitrophenol. (a) p-Benzoquinone (retention time = 8,200 min), (b) hydroquinone (retention time = 14,590 min), (c) p-aminophenol (retention time = 14,705 min), (d) p-nitrophenol (retention time = 18,465 min).

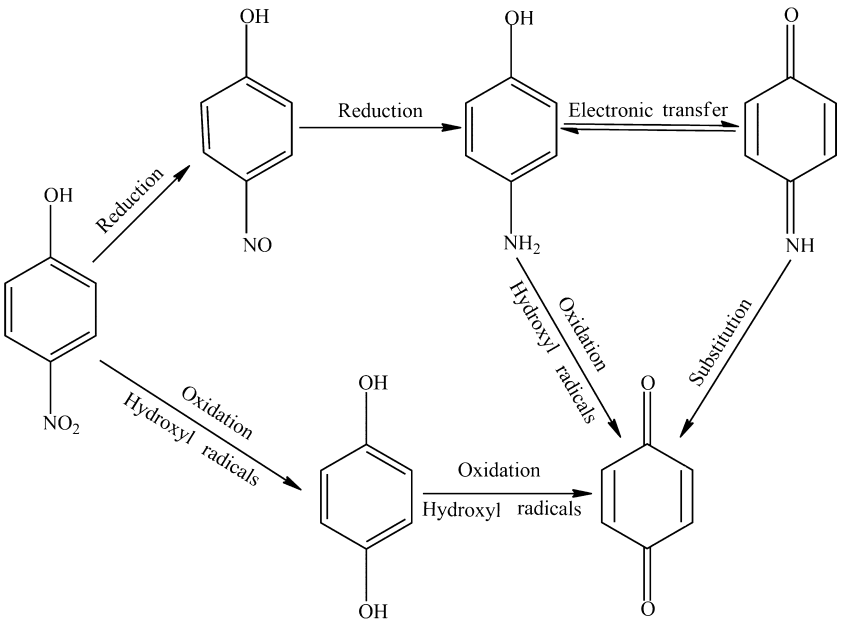

Fig. 9. Proposed degradation pathway for PNP by treated with nZVI/SBA-15. Reaction conditions: 600 mg/L PNP removed on nZVI/SBA-15 with concentration of 5 g/L at 25 °C, 150 rpm, within 240 min.

(C–OH, C–O–R, BE = 286.2 eV), and carbon coordinated to quinone group (C=O, BE = 288 eV) [41]. Compared to the pure nZVI/SBA-15, the treated composites showed another peak of cure-fitting corresponding to C–N (BE = 285.3 eV), consistent with the conclusion gained by Fig. 6a [42].

3.5. Proposed reaction pathway for degradation of PNP

To find out the main mechanisms for the degradation of PNP by nZVI/SBA-15 materials, various intermediates in treatment effluent were detected by a gas chromatography–mass spectrometry (GC/MS), and the results were shown in Figs. 7 and 8. Except the target pollutant, PNP (18.465 min), the identified intermediates included p-aminophenol (14.705 min), hydroquinone (14.590 min), p-benzoquinone (8.200 min) and some unknown compounds or impurities. According to gas chromatogram (Fig. 7), p-aminophenol was the main product in PNP degradation process. However, the p-nitrosophenol was not detected by GC/MS analysis possibly due to its reduction into p-aminophenol instantaneously in the degradation process [43]. Nevertheless, the p-nitrosophenol should participate in the degradation pathway according to the previous studies [43]. What's more, there was no definite evidence indicating the presence of chain product, which revealed that the ring opening reaction almost did not occur in the treatment process.

According to the previous studies [44,45], the degradation pathway of PNP by nZVI/SBA-15 was similar to that by electrochemical system. However, the degradation process could not be accelerated by the monometallic system. So the main degradation pathways were proposed in Fig. 9. For one thing, PNP was reduced to p-nitrosophenol by direct reduction on the surface of composites or indirect reduction of $[H]_{abs}$, then further reduced to p-aminophenol, confirming XPS analysis. Then p-aminophenol was oxidized to p-benzoquinone by hydroxyl [44,45]. Notably, due to the electronic transfer (redox reaction), p-aminophenol might also become p-benzoquinoneimine under acidic condition. In following substitution reaction, p-benzoquinoneimine reacted with H_2O to form p-benzoquinone and ammonia at last [46]. Unfortunately, p-benzoquinoneimine could not be detected owing to the low content and its instability. For another, PNP was oxidized to hydroquinone and then produced p-benzoquinone by hydroxyl radical [45]. In our study, the ring opening reaction of p-benzoquinone almost did not occur, which could be interpreted in a way that the amount of the generated hydroxyl radicals was inadequate for the ring opening reaction due to the limited immobilized quantity of metallic iron. Thus, the PNP degradation process could be proposed as a reduction, accompanied by slight oxidation. According to the previous studies [43,44], obviously, these products exhibited the lower toxicity than their parent compound. Therefore, this degradation process is considered to be a cost-effective pretreatment method for the refractory PNP wastewater [44].

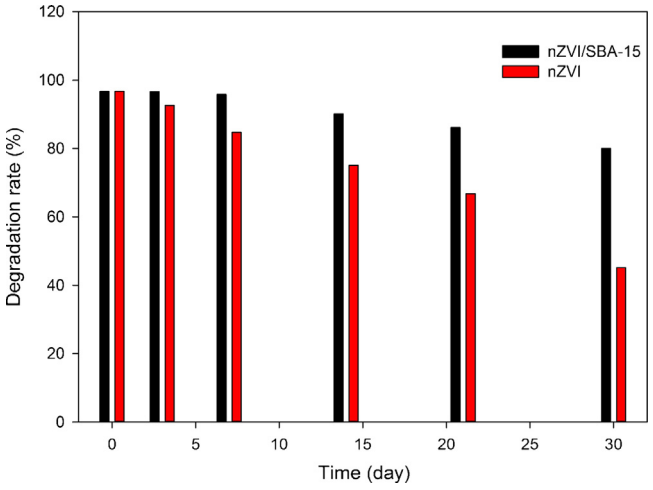

Fig. 10. Effect of exposure time to air on the PNP degradation rate by nZVI/SBA-15 and nZVI. Reaction conditions: 400 mg/L PNP removed on nZVI/SBA-15 and nZVI with concentration of 5 g/L at 25 °C, 150 rpm, within 240 min.

3.6. Antioxidation ability of nZVI/SBA-15

Fig. 10 showed that PNP removal efficiency by nZVI/SBA-15 was still higher than 90% after 14 days' exposure and then declined to 80% after a month's exposure. In order to highlight the antioxidation ability of nZVI/SBA-15, bare nZVI was studied under the same conditions. And results showed that the PNP degradation rate by

nZVI reduced to 75% after 14 days' exposure and finally reached 45% after a month. Apparently, nZVI/SBA-15 was superior to bare nZVI in terms of antioxidation ability. The results could be explained by the fact that nanoscale zero-valent iron particles of the composites were partially inserted into mesoporous silica channels as shown in the TEM images (Fig. 1c insert), which reduced the surface of iron particles contacting with oxygen and protected their activity. Therefore, nZVI/SBA-15 maintained more activity in the PNP degradation under the same exposure condition.

4. Conclusions

In this work, nZVI particles immobilized on mesoporous silica were successfully synthesized and used to degrade PNP in the wastewater. In TEM images of nZVI/SBA-15 composites, some ultrasmall nanoparticles were presented. The composite showed an effective PNP degradation performance, by combining dual functions of reduction and slight oxidation. The solution pH posed an obvious impact on the PNP removal, and the optimum value was pH 3. Removal rate was also affected by the competition of PNP and its intermediate products. Besides, the equilibrium of PNP degradation was reached just in 5 min. The experimental data were fitted well by the pseudo-first-order kinetic model. XPS analysis confirmed that metallic iron disappeared after treating PNP, and some new nitrogen functional groups emerged on the surface of nZVI/SBA-15. According to the intermediate analysis by GC/MS, the composite could degrade PNP into several products with low toxicity. What's more, compared with the bare nZVI, the composite exhibited superior antioxidation ability. Therefore, the above results could provide an appropriate way to remove PNP from water in industrial practice.

Acknowledgements

The study was financially supported by the Young Top-Notch Talent Support Program of China (2012), the National Natural Science Foundation of China (51222805), the Program for New Century Excellent Talents in University from the Ministry of Education of China (NCET-11-0129), Interdisciplinary Research Project of Hunan University, the Fundamental Research Funds for the Central Universities, Hunan University, Foundation for the Author of Excellent Doctoral Dissertation of Hunan Province, and Hunan Provincial Innovation Foundation For Postgraduate (CX2009B080).

References

[1] B. Petroval, T. Budinova, B. Tsyntsarski, V. Kochkodan, Z. Shkavro, N. Petrov, Removal of aromatic hydrocarbons from water by activated carbon from apricot stones, Chem. Eng. J. 165 (2010) 258–264.
[2] Y.-S. Keum, Q.X. Li, Reduction of nitroaromatic pesticides with zero-valent iron, Chemosphere 54 (2004) 255–263.
[3] X.-E. Shen, X.-Q. Shan, D.-M. Dong, X.-Y. Hua, G. Owens, Kinetics and thermodynamics of sorption of nitroaromatic compounds to as-grown and oxidized multiwalled carbon nanotubes, J. Colloid Interface Sci. 330 (2009) 1–8.
[4] M.A.J. Harrison, S. Barra, D. Borghesi, D. Vione, C. Arsene, R.I. Olariu, Nitrated phenols in the atmosphere: a review, Atmos. Environ. 39 (2005) 231–248.
[5] J. Hawari, A. Halasz, S. Beaudet, L. Paquet, G. Ampleman, S. Thiboutot, Biotransformation wastewater by using pulse electro-coagulation process with Fe electrode, Chem. Eng. J. 169 (2011) 84–90.
[6] P. Yang, A.-D. Xu, J. xia, H.-L. Xing, X.-M. Zhang, S.-Y. Wei, N.-N. Wang, Facile synthesis of highly catalytic activity Ni–Co–Pd–P composite for reduction of the p-nitrophenol, Appl. Catal. A 470 (2014) 89–96.
[7] O. Gimeno, M. Carbajo, F.J. Beltran, F.J. Rivas, Phenol and substituted phenols AOPs remediation, J. Hazard. Mater. B 119 (2005) 113–123.
[8] S.W. Peretti, C.J. Tompkins, J.L. Goodall, A.S. Michaels, Extraction of 4-nitrophenol from 1-octanol into aqueous solution in a hollow fiber liquid contactor, J. Membr. Sci. 195 (2001) 193–202.
[9] M.H. Entezari, T. Rohani Bastami, Influence of ultrasound on cadmium ion removal by sorption process, Ultrason. Sonochem. 15 (2008) 428–432.
[10] Y.J. Wu, L.N. Geng, X.R. Wang, R.F. Chen, Y. Wei, D. Wu, Reductive transformation of p-nitrophenol by Fe(II) species: the effect of anionic media, J. Hazard. Mater. 263 (2013) 556–561.
[11] B. Lai, Y.-H. Zhang, R. Li, Y.-X. Zhou, J.L. Wang, Influence of operating temperature on the reduction of high concentration p-nitrophenol (PNP) by zero valent iron (ZVI), Chem. Eng. J. 249 (2014) 143–152.
[12] R. Rangsivek, M.R. Jeke, Removal of dissolved metals by zero-valent iron (ZVI): kinetics, equilibriua, processes and implications for stormwater runoff treatment, Water Res. 39 (2005) 4153–4163.
[13] S.H. Joo, D. Zhao, Destruction of lindane and atrazine using stabilized iron nanoparticles under aerobic and anaerobic conditions: effects of catalyst and stabilizer, Chemosphere 70 (2008) 349–359.
[14] W.Z. Yin, J.H. Wu, P. Li, X.D. Wang, N.W. Zhu, P.X. Wu, B. Yang, Experimental study of zero-valent iron induced nitrobenzene reduction in groundwater: the effects of pH, iron dosage, oxygen and common dissolved anions, Chem. Eng. J. 184 (2012) 198–204.
[15] R.A. Crane, T.B. Scott, Nanoscale zero-valent iron: future prospects for an emerging water treatment technology, J. Hazard. Mater. 211-212 (2012) 112–125.
[16] E. Petala, K. Dimos, A. Douvalis, T. Bakas, J. Tucek, R. Zbřoil, M.A. Karakassides, Nanoscale zero-valent iron supported on mesoporous silica: characterization and reactivity for Cr(VI) removal from aqueous solution, J. Hazard. Mater. 261 (2013) 295–306.
[17] T. Phenrat, N. Saleh, K. Sirk, R.D. Tilton, G.V. Lowry, Aggregation and sedimentation of aqueous nanoscale zerovalent iron dispersions, Environ. Sci. Technol. 41 (2007) 284–290.
[18] X.S. Lv, J. Xu, G.M. Jiang, X.H. Xu, Removal of chromium(VI) from wastewater by nanoscale zero-valent iron particles supported on multiwalled carbon nanotubes, Chemosphere 85 (2011) 1204–1209.
[19] Z.H. Li, H.K. Jones, P.F. Zhang, R.S. Bowman, Chromate transport through columns packed with surfactant-modified zeolite/zero-valent iron pellets, Chemosphere 68 (2007) 1861–1866.
[20] H.J. Zhu, Y.F. Jia, X. Wu, H. Wang, Removal of arsenic from water by supported nano zero-valent iron on activated carbon, J. Hazard. Mater. 172 (2009) 1591–1596.
[21] T. Shahwan, C. Uzum, A.E. Eroğlu, I. Lieberwirth, Synthesis and characterization of bentonite/iron nanoparticles and their application as adsorbent of cobalt ions, Appl. Clay Sci. 47 (2010) 257–262.
[22] X.F. Ling, J.S. Li, W. Zhu, Y.Y. Zhu, X.Y. Sun, J.Y. Shen, W.Q. Han, L.J. Wang, Synthesis of nanoscale zero-valent iron/ordered mesoporous carbon for adsorption and synergistic reduction of nitrobenzene, Chemosphere 87 (2012) 655–660.
[23] X. Sun, H.X. Yu, D. Zheng, X.S. Wang, J.S. Li, L.J. Wang, Incorporation of nanoscale zero-valent iron particles inside the channels of SBA-15 silica rods by a two solvent reduction technique, Appl. Surf. Sci. 279 (2013) 1–6.
[24] X. Sun, Y.B. Yan, J.S. Li, W.Q. Han, L.J. Wang, SBA-15-incorporated nanoscale zero-valent iron particles for chromium (VI) removal from groundwater: mechanism, effect of pH, humic acid and sustained reactivity, J. Hazard. Mater. 266 (2014) 26–33.
[25] E. Delahaye, V. Escax, N.E.I Hassan, A. Davidson, "Nanocasting": using SBA-15 silicas as hard templates to obtain ultrasmall monodispersed γ-Fe_2O_3 nanoparticles, J. Phys. Chem. B 110 (2006) 26001–26011.
[26] J.V. Meer, I. Bardez-Giboire, C. Mercier, B. Revel, A. Davidson, R. Denoyel, Mechanism of metal nanoparticle loading in SBA-15 by the double solvent technique, J. Phys. Chem. C 114 (2010) 3507–3515.
[27] J.V. Meer, I. Bardez, F. Bart, P.-A. Albouy, sion of Co_3O_4 nanoparticles within SBA-15 using alkane solvent, Microporous Mesoporous Mater. 118 (Dispe) (2009) 183–188.
[28] D. Zhao, Q. Huo, J. Feng, B.F. Chmelka, G.D. Stucky, Nonionic triblock and star diblock copolymer and oligomeric surfactant synthese of highly ordered, hydrothermally stable, mesoporous silica structures, J. Am. Chem. Soc. 120 (1998) 6024–6036.
[29] T.R. Bastami, M.H. Entezari, Activated carbon from carrot dross combined with magnetite nanoparticles for the efficient removal of p-nitrophenol from aqueous solution, Chem. Eng. J. 210 (2012) 510–519.
[30] B. Lai, Z.Y. Chen, Y.X. Zhou, P. Yang, J.L. Wang, Z.Q. Chen, Removal of high concentration p-nitrophenol in aqueous solution by zero valent iron with ultrasonic irradiation (US-ZVI), J. Hazard. Mater. 250–251 (2013) 220–228.
[31] G.M. Zeng, Y.Y. Liu, L. Tang, G.D. Yang, Y. Pang, Y. Zhang, Y.Y. Zhou, Z. Li, M.Y. Li, M.Y. Lai, X.X. He, Y.B. He, Enhancement of Cd (II) adsorption by polyacrylic acid modified magnetic mesoporous carbon, Chem. Eng. J. (2014) 115, http://dx.doi.org/10.1016/j.cej.2014.07.
[32] L. Tang, G.-D. Yang, G.-M. Zeng, Y. Cai, S.-S. Li, Y.-Y. Zhou, Y. Pang, Y.-Y. Liu, Y. Zhang, B. Luna, Synergistic effect of iron doped ordered mesoporous carbon on adsorption-coupled reduction of hexavalent chromium and the relative mechanism study, Chem. Eng. J. 239 (2014) 114–122.
[33] L. Tang, Y. Cai, G.D. Yang, Y.Y. Liu, G.M. Zeng, Y.Y. Zhou, S.S. Li, J.J. Wang, S. Zhang, Y. Fang, Y.B. He, Cobalt nanoparticles-embedded magnetic ordered mesoporous cabon for highly effective adsorption of rhodamine B, Appl. Surf. Sci. 314 (2014) 746–753.
[34] J. Dong, Y.S. Zhao, R. Zhao, R. Zhou, Effects of pH and particles size on kinetics of nitrobenzene reduction by zero-valent iron, J. Environ. Sci. 22 (11) (2010) 1741–1747.
[35] L.-N. Shi, X. Zhang, Z.-L. Chen, Removal of chromium (VI) from wastewater using bentonite-supported nanoscale zero-valent iron, Water Res. 45 (2011) 886–892.

[36] B. Lai, Y.X. Zhou, H.K. Qin, C.Y. Wu, C.C. Pang, Y. Lian, J.X. Xu, Pretreatment of wastewater from acrylonitrile-butadiene-styrene (ABS) resin manufacturing by microelectrolysis, Chem. Eng. J. 179 (2012) 1–7.
[37] P.P. Huang, Z.F. Ye, W.M. Xie, Q. Chen, J. Li, Z.C. Xu, M.S. Yao, Rapid magnetic removal of aqueous heavy metals and their relevant mechanisms using nanoscale zero valent iron (nZVI) particles, Water Res. 47 (2013) 4050–4058.
[38] L. Tang, Y. Fang, Y. Pang, G.M. Zeng, J.J. Wang, Y.Y. Zhou, Y.C. Deng, G.D. Yang, Y. Cai, J. Chen, Synergistic adsorption and reduction of hexavalent chromium using highly uniform polyaniline-magnetic mesoporous silica composite, Chem. Eng. J. 254 (2014) 302–312.
[39] V.K. Gupta, N. Atar, M.L. Yola, Z. Üstündağ, L. Uzun, A novel magnetic Fe@Au core–shell nanoparticles anchored graphene oxide recyclable nanocatalyst for the reduction of nitrophenol compounds, Water Res. 48 (2014) 210–217.
[40] R.V. Siriwardane, J.M. Cook, Interactions of SO_2 with sodium deposited on silica, J. Colloid Interface Sci. 108 (1985) 414–422.
[41] L. Zhou, M.H. Zhou, C. Zhang, Y.H. Jiang, Z.H. Bi, J. Yang, Electro-Fenton degradation of p-nitrophenol using the anodize graphite felts, Chem. Eng. J. 233 (2013) 185–192.
[42] G. Beamson, A. Bunn, D. Briggs, High-resolution monochromated XPS of poly (methyl methacrylate) thin films on a conducting substrate, Surf. Interface Anal. 17 (1991) 105–115.
[43] S.H. Yuan, M. Tian, Y.P. Cui, L. Lin, X.H. Lu, Treatment of nitrophenol by cathode reduction and electro-Fenton methods, J. Hazard. Mater. 137 (2006) 573–580.
[44] B. Lai, Y.H. Zhang, Z.Y. Chen, P. Yang, Y.X. Zhou, J.L. Wang, Removal of p-nitrophenol (PNP) in aqueous solution by the micron-scale iron–copper (Fe/Cu) bimetallic particles, Appl. Catal. B: Environ. 144 (2014) 816–830.
[45] Y.R. Zhang, N. Yang, M. Murugananthan, S. Yoshihara, Electrochemical degradation of PNP at boron-doped diamond and platinum electrodes, J. Hazard. Mater. 244-245 (2013) 195–302.
[46] A.J. Bard, L.R. Faulkner, Electrochemical Methods Fundamentals and Applications, Second ed., Wiley, New York, 2000.